Check for updates

Association reactions in femtosecond laser filaments of hexane studied by time-of-flight mass spectrometry with velocity screening

Akitaka Matsuda, [ID] *[a] Yuya Okumura,[a] Kasumi Hashigaya[a] and Akiyoshi Hishikawa [ID] *[ab]

Femtosecond laser filament-induced reactions in gaseous hexane (C_6H_{14}) are studied by time-of-flight ion mass spectrometry. The neutral products are unambiguously distinguished from species produced by ionization for mass analysis, through velocity screening along the flight tube. In addition to hydrogen-capped polyynes, C_nH_2 (n = 4, 6, 8, 10 and 12), the mass spectrometry reveals hydrocarbon molecules in the mass range of m/z 50–146 that have eluded identification in previous studies. The product distributions, together with their dependence on laser pulse energy and repetition rate, provide insight into the association reaction pathways to hydrogen-capped polyynes and other products by laser filaments.

1 Introduction

Ultrashort strong laser fields ($\sim 10^{13}$–10^{14} W cm^{-2}) provide a powerful means to control chemical reactions by driving electrons with their large electric fields.[1–3] Combined with coherent pulse-shaping techniques, the strong-field reaction control demonstrated its efficacy in unimolecular reactions.[4] Selective bond breaking and rearrangement, and orientation selective ionization were demonstrated with various polyatomic molecules in gas phase such as CO_2,[5,6] OCS,[7,8] H_2O,[9,10] C_2H_2,[11] CH_4,[12] CF_4,[13] methylhalides,[14,15] trifluoro- and trichroloacetone,[16] iodohexane,[17] acetophenone,[18] and orgnometallic molecules.[19] Strong laser pulses have been exploited to manipulate bimolecular reactions between gas-phase atoms[20] and molecules[21] and to intermolecular reactions in clusters.[22,23]

The application to many-body reactions has also been demonstrated using femtosecond laser filaments. Laser filament is a needle-like light-emitting body generated by loose focusing of ultrashort laser pulses into a gas or liquid medium. The field intensity of the order of 10^{13} to 10^{14} W cm^{-2} is maintained over a long distance along the filament as a result of competition between nonlinear focusing and defocusing effects.[24–26] Previous studies identified the generation of nanoparticles and films from gaseous reactants, such as carbon nanospheres from CH_4,[27]

hydrogenated amorphous carbon nanoparticles and films from C_2H_4,[28] as well as metal containing nanoparticles from $Al(CH_3)_3$ and $Al_2Mg(CH_3)_8$,[29] by means of fluorescence/Raman spectroscopy, electron energy loss spectroscopy (EELS) and transmission electron microscopy (TEM). For gaseous hexane C_6H_{14}, association reactions to hydrogen-capped polyynes C_nH_2 (n = 6, 8, 10 and 12) were observed by UV absorption spectroscopy of the products recovered in cooled solvent.[30]

In addition to these studies based on the analysis of the recovered products, several *in situ* studies on laser-filament reactions have been reported. Emission spectroscopy was employed[31,32] to identify the intermediates in laser filaments in a gas mixture of CH_4 and air, where the formation of OH radical is shown to be essential in the chain-branching oxidation reaction in the flame of CH_4 and air mixture.[32] Absorption spectroscopy was exploited to investigate reaction intermediates and products, in particular non-fluorescent molecules in their electronic ground state.[33–35] The formation of O_3,[33] nitrogen oxides,[33–35] CO,[35] and HCN[35] by filamentation in air was identified by UV, visible, and infrared absorption spectroscopy.

In contrast to these optical spectroscopic techniques allowing state-resolved detection of the products, ion-mass spectrometry offers identification of a wide range of products with a high sensitivity. It was first applied to a gaseous sample recovered from the reaction cell after laser irradiation for a few hours, where various carbon hydrates, such as C_2H_2 and C_6H_6 from CH_4,[27] and CO_2 and C_2H_2 from a gas mixture of CO and H_2[36] were observed. Recently, laser filament reactions have been investigated by direct sampling of the products from a reaction chamber into a mass spectrometer.[37,38] The application to the filament reaction in C_2H_4 successfully identified a variety of association reaction products from C_3H_4 to C_7H_7.[38]

[a] *Department of Chemistry, Graduate School of Science, Nagoya University, Furo-cho, Chikusa, Nagoya, Aichi 464-8602, Japan.*
E-mail: matsuda.akitaka.f7@f.mail.nagoya-u.ac.jp,
hishikawa.akiyoshi.z6@f.mail.nagoya-u.ac.jp
[b] *Research Center for Materials Science, Nagoya University, Furo-cho, Chikusa, Nagoya, Aichi 464-8602, Japan*

As demonstrated by these studies, the ion mass spectrometry is powerful in investigating the reaction products and intermediates. On the other hand, obtained mass spectra are often contaminated by the fragmentation of the reaction products by ionization,[39] preventing a clear understanding of the reaction process from the product distributions. This becomes significant when association reactions to a large molecular species are anticipated, as they are often susceptible to dissociation. Since the discrimination of nacent products from species produced by mass analysis is often challenging, a soft ionization technique suppressing extensive fragmentation upon ionization, such as electrospray ionization (ESI) or matrix-assisted laser desorption ionization (MALDI) is employed when applicable.

Here we introduce an alternative approach to distinguish filament products from ionization-induced fragments. The method is based on the difference in initial velocities between filament products and ionization fragments after ionization, which is applied to identify laser-filament reaction products of hexane (C_6H_{14}). The paper is organized as follows. In Section 2, we describe our experimental setup. The filament products are directly sampled into the time-of-flight mass spectrometer, which allows a clear identification of the products and the intermediates to discuss the reaction processes. The velocity-resolved mass spectroscopy is presented in Section 3. Possible reaction pathways for the formation of hydroegen-capped polyynes and other products are discussed, as well as the effects of the laser repetition rate and laser intensity on the product distributions. The results of the present study are summarized in Section 4.

2 Experiment

The experimental setup is similar to that described previously.[38] Briefly, it consists of three sections, a reaction gas cell, a differential pumping stage, and a time-of-flight mass spectrometer (Fig. 1). The output from a Ti:sapphire laser amplifier system (800 nm, 50 fs, 1 kHz) was divided into two by a beamsplitter. The main pulse (98%) was focused into the reaction gas cell by a plano-convex lens (f = 200 mm) to generate a laser filament. The remaining horizontally-polarized pulse (2%) was focused into the mass spectrometer using a plano-convex lens (f = 200 mm), which serves as an ionization probe for the mass analysis of the filament products. Hexane (C_6H_{14}, vapor pressure $\sim$0.2 atm at room temperature) was continuously supplied into the reaction gas cell using Ar as a carrier gas. The gas flow rate was controlled to keep the pressure inside the reaction gas cell at a constant value of 0.4 atm.

After interaction with the laser filaments, the reaction products are introduced into the mass spectrometer as a quasi-continuous molecular beam[38] *via* an orifice (ϕ 200 μm) and a skimmer (ϕ 200 μm) in the differential pumping stage. The filament products ionized by the probe laser pulse are guided by a static electric field to the micro-channel plate detector. Because of the static electric field, ionic species are deflected before entering the flight tube. Therefore the present setup exclusively detects the neutral products from the reaction gas cell.
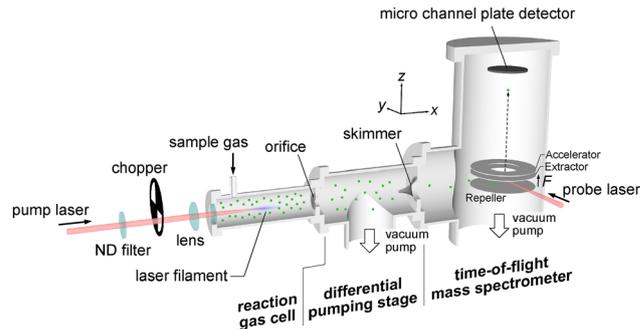

Fig. 1 Schematic of the experimental setup consisting of a reaction gas cell, a differential pumping stage, and a Wiley–McLaren-type time-of-flight (TOF) mass spectrometer. The products of femtosecond laser-filament reactions produced in the reaction gas cell by filament laser (pump) is introduced into the TOF mass spectrometer *via* an oriffice and a skimmer. The products ionized by ionization laser (probe) are guided by electric fields and detected by a microchannel plate detector. The repetition rate and energy of the filament laser are varied by an optical chopper and neutral density filters, respectively.

The field intensity achieved by the probe pulse is estimated to be 8.2×10^{13} W cm^{-2}. The Keldysh parameter $\gamma = \sqrt{I_p/(2U_p)}$, with I_p and U_p being the ionization potential and the poderomotive potential, is less than 1 for $I_p < 10$ eV, suggesting that tunnel ionization dominates the ionization process in the present study. An optical chopper is inserted to the filament laser beam to study the effect of the repetition rate on the product distributions. The pulse energy is varied by neutral density (ND) filters.

3 Results and discussion

3.1 Time-of-flight ion mass spectrometry with velocity screening

Fig. 2(a) shows a time-of-flight mass spectrum of C_6H_{14} obtained without the filamentation laser in the reaction chamber. In addition to the peak at t = 6.7 μs corresponding to the parent ion ($C_6H_{14}^+$), the spectrum shows many peaks at shorter flight times, some of which have peak intensities even larger than that of the parent ion. A similar mass spectrum is observed by electron impact ionization.[40] These additional peaks are assigned to fragment ions produced by the probe pulse for the mass analysis.[41,42] The fragmentation was not significant on ethylene.[38] The marked contrast to the previous study implies that the product distribution of the filament-induced reaction in hexane requires a secure discrimination between the filament products and the probe products.

Under the space-focusing conditions of a time-of-flight mass spectrometer,[43] the spectrum peak width is essentially determined by the distribution of the initial velocity v_z at the time of ionization along the time-of-flight axis (see Fig. 1). The initial velocity of the parent ion ($C_6H_{14}^+$) is governed by the transverse velocity of the molecular beam. On the other hand, the fragment ions produced by the ionization can gain additional velocity due to the kinetic energy released by the fragmentation. This results in a broader velocity distribution than that of the parent ion.

This journal is © the Owner Societies 2026

Phys. Chem. Chem. Phys., 2026, **28**, 2976–2985 | **2977**
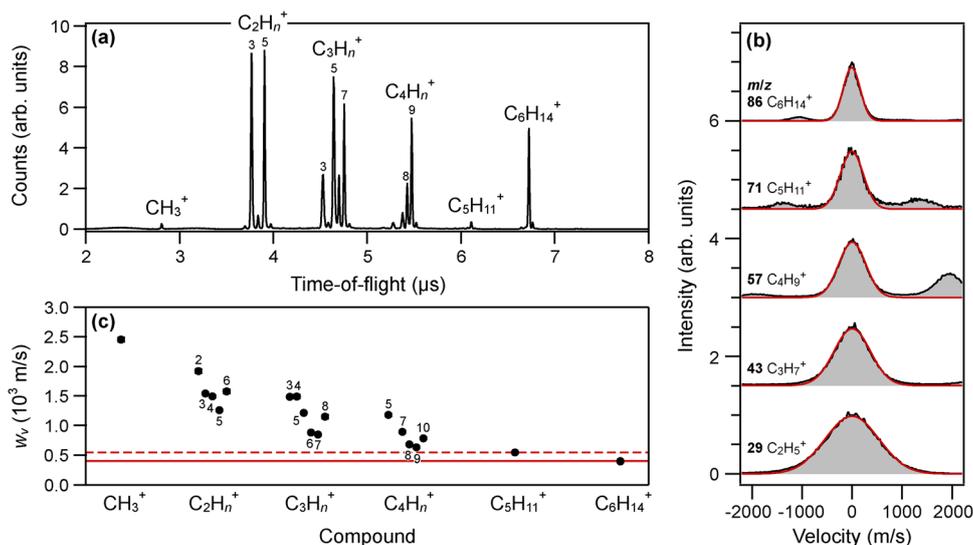
Fig. 2 (a) Time-of-flight spectrum of hexane recorded without the filamentation laser. The field intensity of the ionization laser is estimated to be 8.2×10^{13} W cm^{-2}. Note that the small peak corresponding to m/z 40 is attributed to $C_3H_4^+$ instead of Ar$^+$ from the carrier gas, because the tunnel ionization of Ar is less efficient than the hydrocarbon molecules due to the high ionization potential (15.8 eV). (b) Velocity distribution of representative peaks in (a). Side peaks observed in the velocity distributions for $C_6H_{14}^+$, $C_5H_{11}^+$, and $C_4H_9^+$ are due to ions with neighboring mass, which can be assigned to $^{13}CC5H14$ isotopologue and fragments with different number of hydrogen atoms, such as $C_5H_{12}^+$, $C_5H_{10}^+$, and $C_4H_8^+$, respectively. (c) Full width at the half maximum of the velocity distrubution w_v for the peaks observed in (a). The reference width w_v^0 (solid) and the critical width w_v^c (dashed) are indicated.

Fig. 2(b) shows the velocity distribution along the z-axis for selected ionic species in the time-of-flight spectrum in Fig. 2(a). The v_z component is given as,[44]

$$v_z = \frac{qF_{acc}}{m}(t_0 - t). \tag{1}$$

Here q and m are the electric charge and the mass of the ion, respectively, and F_{acc} is the strength of the electric field in the ion extraction region, t is the flight time, and t_0 is that of the ion with $v_z = 0$. The $C_6H_{14}^+$ parent ion exhibits a narrow velocity distribution, while significantly broader distributions are observed for the fragment ions.

Fig. 2(c) shows the full width at half maximum (FWHM) of the velocity distribution, w_v, obtained for each peak from least-squares fitting to a Gaussian function. The width increases for a smaller fragment, which can be interpreted as a result of heavy fragmentation caused by ionization to highly excited or highly charged states. It is worth noting that a significant difference is seen even in the widths of the parent ion and the largest fragment ion, $C_5H_{11}^+$, showing that the velocity width can be used to discriminate the nascent filament products in the sample from the probe products. In the following, the widths of $C_6H_{14}^+$ and $C_5H_{11}^+$ are adopted as the reference width w_v^0 and the critical width w_v^c, respectively, which are used to identify the filament products from hexane.

3.2 Laser-filament product distributions

Fig. 3(a) shows the time-of-flight mass spectrum obtained with a filament laser operated at 480 μJ per pulse and a repetition rate of 500 Hz. The mass spectrum looks similar to that observed without the filament laser. However, the enlarged spectrum in
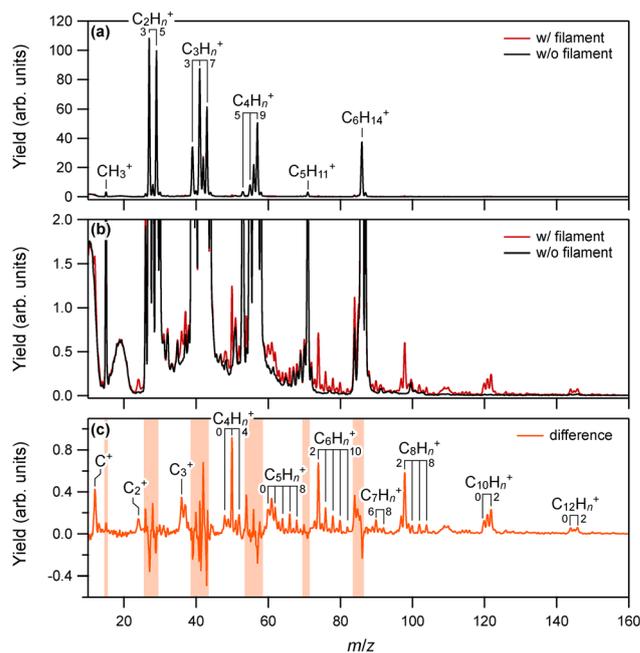

Fig. 3 (a) Mass spectra obtained with (red) and without (black) the filament laser pulse (pulse energy: 480 μJ, repetition rate: 500 Hz). Each spectrum is normalized at m/z 29. Fragment ions generated from the parent C_6H_{14} molecule solely by the probe pulse are mainly observed. (b) Expanded view of the mass spectra shown in (a). (c) Difference spectrum between the spectra obtained with and without the filamentation laser pulse. The hatched areas indicate spectral regions where strong signals of the probe products from hexane hinder clear identification of the filament products.

Fig. 3(b) reveals the emergence of new peaks in the spectral range from m/z 10 to 150. The new peaks are more clearly visible in the difference between the spectra recorded with and without the filament (Fig. 3(c)). Hydrogen-capped polyynes $C_nH_2^+$ (n = 6, 8, 10, 12) observed in the previous study by UV absorption spectroscopy of recovered samples[30] are observed. In addition, the time-of-flight mass spectrometry identifies a number of hydrocarbon molecules as assigned in Fig. 3(c). The broad widths of the peaks around m/z 110 hinder clear assignments, but they could be attributed to $C_9H_n^+$ (n = 1, 2).

Fig. 4 plots the full widths at the half maximum w_v of peaks identified in the difference spectrum in Fig. 3(c). The velocity distributions of selected species are displayed as insets in Fig. 4. Some species such as $C_4H_3^+$, $C_5H_8^+$, $C_6H_{10}^+$, $C_7H_8^+$, $C_8H_8^+$, and $C_{10}H_2^+$, have narrow widths comparable with the hexane cation ($C_6H_{14}^+$). On the other hand, the peak of C_4H^+, for example, exhibited a significantly broader width.

Under the present quasi-continuous free-expansion conditions, the fragment products are entrained by the carrier gas to the mass spectrometer. This implies that all the products formed in laser filaments have velocity distributions similar to those of the dominant species of the beam, $i.e.$, C_6H_{14} and Ar, in the present case. Therefore, the reference and critical widths, w_v^0 and w_v^c, determined in the previous section for C_6H_{14} can be used to discriminate the filament products from the probe products. Namely, peaks with widths w_v that satisfy $w_v < w_v^c$ are attributed to filament products, whereas those with $w_v \geq w_v^c$ are classified as probe products.

Fig. 4 shows that mass peak heavier than $C_6H_{14}^+$, such as $C_8H_n^+$, $C_{10}H_n^+$ and $C_{12}H_n^+$ are assigned to filament reaction products, while those lighter than $C_6H_{14}^+$ are mostly formed by fragmentation, except for $C_4H_n^+$ (n = 2 and 3) and $C_5H_n^+$ (n = 6 and 8). In principle, each mass peak could contain contributions from both the filament product and the probe product. The resultant peak profile in such a case would consist of narrow and broad components. However, since the velocity distributions are well expressed by single Gaussian profiles as plotted in the insets of Fig. 4, the observed species are attributed to either of the two possible origins.

Fig. 5(a) shows the integrated intensities of the peaks observed in the difference spectrum in Fig. 3. For a more quantitative discussion of the distribution of the filament products, the ionization efficiency of each species should be taken into account.[38] As mentioned above, the ionization should be well described by tunnel ionization under the present experimental conditions. The ionization rate can be evaluated by the Ammosov-Delone-Krainov (ADK) theory,[45,46] using the ionization potentials as described in the previous study[38] (see also Supplementary Information). Here the structure factor describing the effect of molecular orientation to the laser electric field is not considered for simplicity. Fig. 5(a) also shows the ionization probability P calculated for each species in the spectrum, by time integration of the tunnel rate over the ionization pulse, where a Gaussian intensity profile is assumed for the ionization laser pulse.

The relative peak intensity of each compound in Fig. 5(a) is divided by the corresponding ionization efficiency S, which accounts for variations in the ionization probability P near the focal spot.[38] The resultant relative yield distribution is shown in Fig. 5(b). Here the relative ratio of the peak width $r_v = w_v/w_v^0$ is used to distinguish the filament products ($r_v < r_v^c$) and the probe
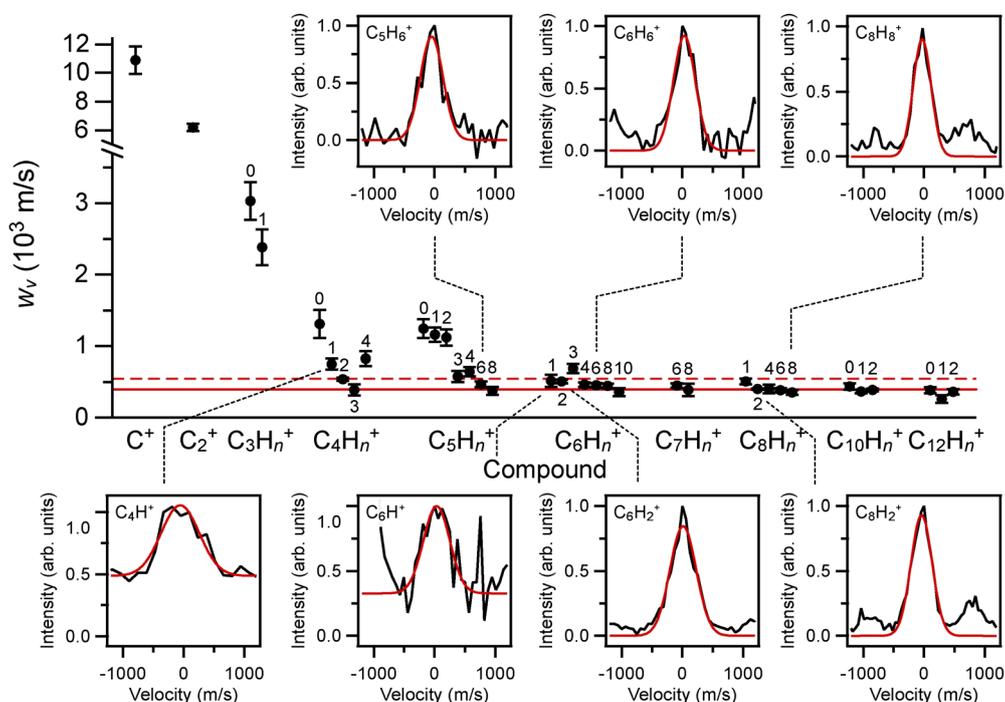

Fig. 4 Full-width half maximum of the velocity distrubution of the major peaks observed in the difference spectrum. The velocity distribution of selected peaks are also shown. The horizontal lines represent the reference width w_v^0 and critical width w_v^c, respectively.
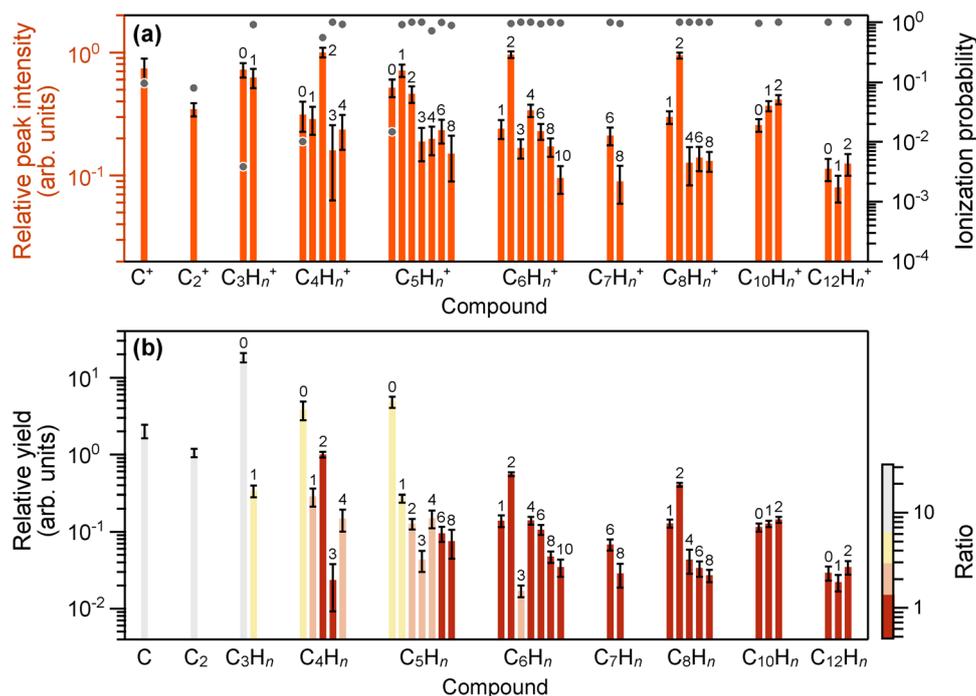
Fig. 5   (a) Relative yields of the peaks observed in Fig. 3(c). The number of hydrogen atoms (n) is indicated above each bar. Tunnel ionization probabilities calculated for the probe pulse with a duration of 50 fs and a peak intensity of 8.2×10^{13} W cm^{-2} are also shown. (b) Relative yields of the products obtained after tunnel ionization efficiency correction. Since the ionization energies of C_nH (n = 4, 6, 8, 10, 12) are unavailable, the ionization potentials are assumed to be the same as that of C_nH_2. The color indicates the ratio $r_v = w_v/w_v^0$ of each peak with w_v^0 being the reference width determined from the $C_6H_{14}^+$ peak. The filament products ($r_v < r_v^c$) are distiguished from the probe products ($r_v \geq r_v^c$).

products ($r_v \geq r_v^c$), where $r_v^c = w_v^c/w_v^0$ is the ratio between the critical and reference widths defined in the previous section. The product distribution spectrum with $r_v \lesssim r_v^c$ shows that the hydrogen-capped polyynes, C_nH_2 with n = 4, 6, 8, 10 and 12 are formed and that the smaller polyynes with n = 4, 6, 8, are the major products from the filament. The yields decrease as the number of included carbon atoms increases. A similar spectrum is obtained at a lower ionization pulse intensity of 5.0×10^{13} W cm^{-2} (see Supplementary Information), showing that it is not sensitive to the ionization pulse intensity under the present experimental conditions.

3.3   Effects of filament laser parameters

3.3.1   Repetition rate. As the repetition rate of the filament laser pulse increases, the time interval of laser irradiation would become shorter or comparable to the timescale of unimolecular decay or diffusion of reaction products. This leads to an accumulation of reaction intermediates subjected to irradiation of subsequent filament laser pulses.[47,48] Indeed, previous studies of laser filamentation in air showed that laser energy absorption by the laser filament at higher repetition rate (1 kHz) becomes considerably larger than at lower repetition rates (1–10 Hz).[49] This was attributed to the electronically excited molecules formed in the metastable states in laser filaments that undergo ionization by subsequent laser pulses.

Fig. 6 plots the repeptition rate dependence of the yields of the hydrogen-capped polyyne, C_nH_2 (n = 4, 6, 8, 10 and 12). The
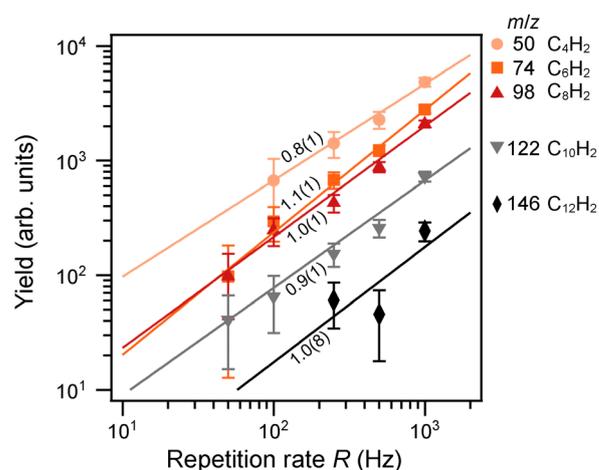

Fig. 6   Repetition-rate dependence of the molecular yields per unit time for hydrogen-capped polyynes C_nH_2 (n = 4, 6, 8, 10, 12) with m/z 50, 74, 98, 122, and 146, obtained at the filament laser energy of 300 μJ per pulse. The solid lines show the curve fitting results to a power function R^{k_r}, where R is the repetition rate. The numbers denote the nonlinear coefficients k_r.

least-squares fitting to a power function of the repetition rate R^{k_r} shows that the yields depend linearly ($k_r \sim 1$) with the repetition rate R, regardless of the products. This shows that the observed filament reactions are induced by single laser pulses.

3.3.2   Pulse energy. Laser pulse energy can be another important parameter in laser filament induced reactions. For an isolated molecule, the fragmentation is expected to become
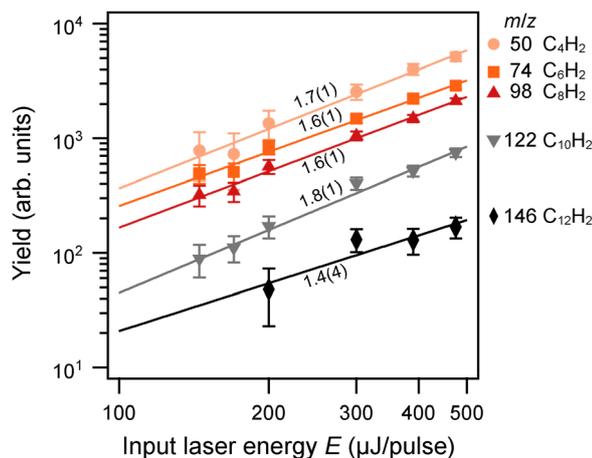
2980 | *Phys. Chem. Chem. Phys.*, 2026, **28**, 2976–2985

This journal is © the Owner Societies 2026

Fig. 7 Filamentation laser-energy dependence of the molecular yields for hydrogen-capped polyynes C_nH_2 (n = 4, 6, 8, 10 and 12), obtained at the repetition rate of 500 Hz. The solid line shows the curve fitting results to a power function E^{k_e}, with E being the pulse energy. The numbers denote the nonlinear coefficients k_e.

significant as the pulse energy increases, as a result of nonlinear excitation and ionization in strong laser fields. In the previous study, it was shown that the product distribution of the laser filament reaction in ethylene is sensitive to the laser pulse energy.[38] Fig. 7 shows the yields of the hydrogen-capped polyynes plotted as a function of the pulse energy E of the filamentation laser. The pulse energy dependence is well expressed by E^{k_e}, with k_e being the nonlinear coefficient. Interestingly, these products have similar values $k_e \sim 1.7$, showing that the product distribution does not vary significantly by pulse energy. This can be interpreted in terms of the intensity clamping effect in a filament. Because of the balance between the nonlinear focusing and defocusing, the laser field intensity is maintained at $\sim 1 \times 10^{14}$ W cm^{-2} in a laser filament.[24–26,50] Instead, the increase of input energy results in the increase of filament volume.[51,52] Therefore the product yields increase as the pulse energy, but with no dependence on the product species in this energy range.

The pulse energy dependence observed in the present study shows a marked contrast to the filament reactions in ethylene. In the latter case, the yields of filament products such as C_5H_n substantially increase with an increase of pulse energy (155 μJ per pulse) by a factor of two, resulting in a substantial difference in the product distribution.[38] This may be attributed to the difference in the ionization efficiency between these species. Indeed, previous studies of strong field ionization of ethylene[53] show that the ionization yield becomes saturated at a higher field intensity ($\sim 1 \times 10^{14}$ W cm^{-2}) than that of hexane ($\sim 6 \times 10^{13}$ W cm^{-2}),[41] though their ionization potentials are similar (10.5 eV for ethylene and 10.1 eV for hexane[54]). This implies that the filament clamping intensity for ethylene can be higher than that for hexane, which would explain the difference in the pulse energy dependence of the product distribution between hexane and ethylene.

3.4 Association reactions in femtosecond laser filaments of hexane

As discussed in the previous subsection, the filament reactions in the present study are induced by a single laser pulse. The products with masses smaller than hexane (m/z 86) could be formed by the fragmentation of the parent molecule in the laser filament. Indeed, the mass spectrum of hexane presented in Fig. 3(a) shows that various fragment ions formed at a field intensity (8.2 × 10^{13} W cm^{-2}) close to the clamp intensity of a filament ($\sim 1 \times 10^{14}$ W cm^{-2}). This in turn suggests that neutral fragments observed in the present study could be produced in the filaments as their counterparts. For example, neutral products C_4H_{14-n} could be produced as the counterpart of $C_2H_n^+$ (n = 1–6) observed in Fig. 3, if they are produced by two-body fragmentation of the parent ion, $C_6H_{14}^+$. The absence of these neutral species, C_4H_8, C_4H_9, C_4H_{10}, C_4H_{11}, C_4H_{12} and C_4H_{13}, in Fig. 5 suggests that they are formed either by more substantial fragmentation of the parent ion through, *e.g.*, a three-body dissociation or possibly by association reactions of smaller fragments. This applies to other small neutral species observed in the present study.

The neutral products larger than hexane could be formed by association reactions between the filament reaction products. Reactions of small hydrogen-deficient hydrocarbon radicals with other hydrocarbons have been extensively studied because of their importance in the formation of large carbonaceous molecules such as polycyclic aromatic hydrocarbons, fullerenes, and soot.[55–63]

The butadiynyl radical (C_4H), which has attracted attention due to its abundance in interstellar molecular clouds and comets, has been proposed to undergo hydrogen abstraction reactions with saturated hydrocarbons, $C_4H + C_nH_{2n+2}$ (n = 1–4) $\rightarrow C_4H_2 + C_nH_{2n+1}$, to form CH_3, C_2H_5, C_3H_7, and C_4H_7.[57] The reactions with unsaturated hydrocarbon molecules, *e.g.*, $C_4H + C_4H_6 \rightarrow C_8H_6 + H$, were also proposed. As for the polyynes, recent experiments[56,59–62] show that the chain length of polyynes can be extended by reactions with C_nH (n = 1–8). The C_4H radical can contribute to the formation of larger polyynes, such as C_8H_2, $C_{10}H_2$, and $C_{12}H_2$, through the reactions $C_4H + C_4H_2 \rightarrow C_8H_2 + H$,[61] $C_4H + C_6H_2 \rightarrow C_{10}H_2 + H$,[62] and $C_4H + C_8H_2 \rightarrow C_{12}H_2 + H$,[55] respectively.

However, the velocity-screened product spectrum in Fig. 5(b) shows that C_4H is not produced as a filament product, which would otherwise appear as a narrow peak at m/z 49 in the mass spectra.[64] This suggests that the pathways involving C_4H have minor contributions to the association reactions in laser filaments. Instead, the C_6H radical observed in the product spectrum implies other pathways leading to $C_{10}H_2$ by $C_6H + C_4H_2 \rightarrow C_{10}H_2 + H$ and to $C_{12}H_2$ by $C_6H + C_6H_2 \rightarrow C_{12}H_2 + H$[55] as both C_4H_2 and C_6H_2 are observed in the spectrum. Further investigation of these reaction pathways is needed, but previous studies of closely related systems involving C_4H radicals reacting with small polyynes indicate that radical-addition to C_4H_2 and C_6H_2 would be essentially barrier-less reactions readily leading to to chain growth of polyynes. Another pathway was

suggested to form a smaller polyyne C_8H_2 *via* $C_6H + C_2H_2 \rightarrow C_8H_2 + H$,[59] though C_2H_2 is not confirmed as the product by the present study due to the overlap with the probe product $C_2H_2^+$ from hexane (see Fig. 3). The previous crossed-beam studies also show that hydrogen-capped polyynes containing an odd number of carbon atoms can be formed, for example, by $C_3H + C_6H_2 \rightarrow C_9H_2 + H$.[62] However, the product spectrum (Fig. 5) obtained shows that C_9H_2 is not produced in the present study. This is consistent with the absence of C_3H in the product spectrum after the velocity discrimination.

Association reaction with metastable $C_4H_2^*$ can be another reaction routes to polyynes as discussed in a gas flow reaction study.[65] For example, C_8H_2 was identified as a reaction product between $C_4H_2^*$ and C_4H_2.[65] Since the peak with m/z 50 identified in Fig. 5 can be assigned to both C_4H_2 and $C_4H_2^*$, such reaction may contribute in forming C_8H_2. The formation of C_7H_6 was also observed in the reaction between $C_4H_2^*$ with C_3H_6, which may also contribute in forming products other than hydrogen capped polyynes in the present study. Unfortunately, C_3H_6 is not confirmed as a filament product in the present study, as the mass peak overlaps with $C_3H_6^+$ formed by the dissociative ionization of hexane by the ionization laser pulse.

Anionic intermediates, which evade observation by the present experimental setup, may also contribute to the product distribution. It was reported[66] that negative ions are formed in aerial laser filament. In the present case, C_6H^- might be formed in the filament because of the large electron affinity (3.8 eV).[67] The previous crossed beam experiments have shown that C_6H^- would react with C_2H_2 to form C_8H^-, $C_6H^- + C_2H_2 \rightarrow C_8H^- + H_2$,[68] which may undergo subsequent reactions such as ion–ion recombination or ion-neutral associative detachment[69] to form neutralized C_8H_2. The contributions from such anionic carbon chain growth requires further studies to understand the filament induced reactions.

4 Summary and outlook

The present study demonstrated the time-of-flight mass spectrometry of the products from femtosecond filaments in hexane, where the velocity screening proved to be a powerful approach to securely distinguish the filament neutral products from the probe products. Direct sampling from the reaction cell allows for identification of various intermediates and products, including hydrogen-capped polyynes, C_nH_2 (n = 4, 6, 8, 10 and 12) as well as other hydrocarbon molecules that escaped from identification in the previous studies.

Possible routes to the formation of the hydrogen-capped polyynes in laser filaments are discussed, including collisional reaction among the fragments. The synthesis of hydrogen-capped polyynes C_nH_2 has attracted wide interests in both materials science[70,71] and astrochemistry,[72] where chain growth reactions $C_{2n}H + C_{2m}H_2 \rightarrow C_{2m+2n}H_2 + H$ are proposed to be responsible for the synthesis of polyynes. Present study suggests that C_6H and C_8H radicals or possibly metastable/anionic species play more important roles than C_4H in the filament-induced reactions to

large hydrogen-capped polyynes (n = 8, 10 and 12). Further investigation on the reaction of different molecular species would elucidate the characteristic features of laser filament reactions in more depth.

Strong laser fields offer a unique means of controlling chemical reactions through their electric-field waveforms as discussed in Introduction. In particular, closed-loop optimization employing mass spectrometry provides a powerful approach to tailoring the waveform, with reaction dynamics at each step monitored by product distribution, as previously demonstrated for unimolecular reactions.[18,19] The present velocity-resolved ion mass spectrometry constitutes an ideal tool for optimizing the yields of neutral products, thereby providing a pathway to efficiently control both unimolecular and many-body chemical reactions *via* laser waveform shaping.

Conflicts of interest

There are no conflicts to declare.

Data availability

The data that support the findings of this article are not publicly available upon publication because it is not technically feasible and/or the cost of preparing, depositing, and hosting the data would be prohibitive within the terms of this research project. The data are available from the authors upon reasonable request.

Supplementary information (SI) is available. See DOI: https://doi.org/10.1039/d5cp03867g.

Acknowledgements

References

1 B. J. Sussman, D. Townsend, M. Y. Ivanov and A. Stolow, Dynamic Stark control of photochemical processes, *Science*, 2006, **314**, 278–281.

2 M. E. Corrales, J. González-Vázquez, G. Balerdi, I. R. Solá, R. de Nalda and L. Bañares, Control of ultrafast molecular photodissociation by laser-field-induced potentials, *Nat. Chem.*, 2014, **6**, 785–790.

3 K. I. Hilsabeck, J. L. Meiser, M. Sneha, J. A. Harrison and R. N. Zare, Nonresonant photons catalyze photodissociation of phenol, *J. Am. Chem. Soc.*, 2019, **141**, 1067–1073.

4 D. Goswami, Optical pulse shaping approaches to coherent control, *Phys. Rep.*, 2003, **374**, 385–481.

5 T. Endo, H. Fujise, A. Matsuda, M. Fushitani, H. Kono and A. Hishikawa, Coincidence momentum imaging of asymmetric Coulomb explosion of CO_2 in phase-locked two-color

2982 | *Phys. Chem. Chem. Phys.*, 2026, **28**, 2976–2985

This journal is © the Owner Societies 2026

intense laser fields, *J. Electron Spectrosc. Relat. Phenom.*, 2016, **207**, 50–54.

6   T. Endo, H. Fujise, Y. Kawachi, A. Ishihara, A. Matsuda and M. Fushitani, *et al.*, Selective bond breaking of CO_2 in phase-locked two-color intense laser fields: laser field intensity dependence, *Phys. Chem. Chem. Phys.*, 2017, **19**, 3550–3556.

7   H. Ohmura, N. Saito and T. Morishita, Molecular tunneling ionization of the carbonyl sulfide molecule by double-frequency phase-controlled laser fields, *Phys. Rev. A:At., Mol., Opt. Phys.*, 2014, **89**, 013405.

8   T. Endo, K. M. Ziems, M. Richter, F. G. Fröbel, A. Hishikawa and S. Gräfe, *et al.*, Post-ionization dynamics of the polar molecule OCS in asmmetric laser fields, *Front. Chem.*, 2022, **10**, 859750.

9   E. Kechaoglou, S. Kaziannis and C. Kosmidis, Controlling intramoleculr hydrogen migration by asymmetric laser fields: the water case, *Phys. Chem. Chem. Phys.*, 2019, **21**, 11259–11265.

10 E. Kechaoglou, K. Ferentinou, S. Kaziannis and C. Kosmidis, Exploring the influence of experimental parameters on the interaction of asymmetric $\omega/2\omega$ fields with water isotopologues, *J. Chem. Phys.*, 2021, **154**, 244306.

11 Q. Song, X. Gong, Q. Ji, K. Lin, H. Pan, J. Ding and H. Zeng, *et al.*, Directional deprotonation ionization of acetylene in asymmetric two-color laser fields, *J. Phys. B: At., Mol. Opt. Phys.*, 2015, **48**, 094007.

12 H. Hasegawa, A. Matsuda, T. Morishita, L. B. Madsen, F. Jensen and O. I. Tolstikhin, *et al.*, Dissociative ionization and Coulomb explosion of CH_4 in two-color asmmetric intense laser fields, *Phys. Chem. Chem. Phys.*, 2023, **25**, 25408–25419.

13 H. Hasegawa, T. Walmsley, A. Matsuda, T. Morishita, L. B. Madsen and F. Jensen, *et al.*, Asymmetric dissociative tunneling ionization of tetrafluoromethane in ω-2ω intense laser fields, *Front. Chem.*, 2022, **10**, 857863.

14 H. Ohmura, F. Ito and M. Tachiya, Phase-sensitive molecular ionization induced by a phse-controlled two-color laser field in methyl halides, *Phys. Rev. A:At., Mol., Opt. Phys.*, 2006, **74**, 043410.

15 S. G. Walt, N. B. Ram, A. von Conta, O. I. Tolstikhin, L. B. Madsen and F. Jensen, *et al.*, Role of multi-electron effects in the asymmetry of strong-field ionization and fragmentation of polar molecules: The methyl halide series, *J. Phys. Chem. A*, 2015, **119**, 11772–11782.

16 D. Cardoza, M. Baertschy and T. Weinacht, Understanding learning control of molecular fragmentation, *Chem. Phys. Lett.*, 2005, **411**, 311–315.

17 H. Ohmura, N. Saito, H. Nonaka and S. Ichimura, Dissociative ionization of a large molecule studied by intense phase-controlled laser fields, *Phys. Rev. A:At., Mol., Opt. Phys.*, 2008, **77**, 053405.

18 R. J. Levis, G. M. Menkir and H. Rabitz, Selective bond dissociation and rearrangement with optimally tailored, strong-field laser pulses, *Science*, 2001, **292**, 709–713.

19 A. Assion, T. Baumert, T. B. Bergt, B. Kiefer, V. Seyfried and M. Strehle, *et al.*, Control of chemical reactions by feedback-optimized phase-shaped femtosecond laser pulses, *Science*, 1998, **282**, 919–922.

20 L. Levin, W. Skomorowski, L. Rybak, R. Kosloff, C. P. Koch and Z. Amitay, Coherent control of bond making, *Phys. Rev. Lett.*, 2015, **114**, 233003.

21 J. Ray and T. Seideman, Strong field quantum control of bimolecular reactions, *J. Chem. Phys.*, 2025, **163**, 114302.

22 Y. Mi, E. Wang, Z. Dube, T. Wang, A. Y. Naumov and D. M. Villeneuve, *et al.*, D_3^+ formation through photoionization of the molecular D_2-D_2 dimer, *Nat. Chem.*, 2023, **15**, 1224–1228.

23 L. Zhou, H. Ni, Z. Jiang, W. Jiang, W. Zhang and P. Lu, *et al.*, Ultrafast formation dynamics of D_3^+ from the light-driven bimolecular reaction of the D_2-D_2 dimer, *Nat. Chem.*, 2023, **15**, 1229–1235.

24 S. L. Chin, S. A. Hosseini, W. Liu, Q. Luo, F. Théberge and N. Aközbek, *et al.*, The propagation of powerful femtosecond laser pulses in optical media: physics, applications, and new challenges, *Can. J. Phys.*, 2005, **83**, 863–905.

25 A. Couairon and A. Mysyrowicz, Femtosecond filamentation in transparent media, *Phys. Rep.*, 2007, **441**, 47–189.

26 L. Bergé, S. Skupin, R. Nuter, J. Kasparian and J. P. Wolf, Ultrashort filaments of light in weakly ionized, optically transparent media, *Rep. Prog. Phys.*, 2007, **70**, 1633–1713.

27 S. L. Shumlas, K. M. Tibbetts, J. H. Ohdner, D. A. Romanov, R. J. Levis and D. R. Strongin, Formation of carbon nanospheres via ultrashort pulse laser irradiation of methane, *Mater. Chem. Phys.*, 2015, **156**, 47–53.

28 A. Matsuda, T. Hayashi, R. Kitaura and A. Hishikawa, Femtosecond laser filamentation in gaseous ethylene: formation of hydrogenated amorphous carbon, *Chem. Lett.*, 2017, **46**, 1426–1429.

29 K. M. Tibbetts, J. Odhner, S. Vaddypally, B. Tangeysh, E. B. Cerkez and D. R. Strongin, *et al.*, Amorphous aluminum-carbide and aluminum-magnesium-carbide nanoparticles from gas phase activation of trimethylaluminum and octamethyldialuminummagnesium using simultaneous spatially and temporally focused ultrashort laser pulses, *Nano-Struct. Nano-Objects*, 2016, **6**, 1–4.

30 Y. Taguchi, H. Endo, T. Kodama, Y. Achiba, H. Shiromaru and T. Wakabayashi, *et al.*, Polyyne formation by ns and fs laser induced breakdown in hydrocarbon gas flow, *Carbon*, 2017, **115**, 169–174.

31 H. Xu, R. Li and S. L. Chin, Photoemission mechanisms of methane in intense laser fields, *Chin. Opt. Lett.*, 2015, **13**, 070007.

32 H. Zang, H. Li, Y. F. Zhang, S. Chen, H. Xu and R. Li, Robust and ultralow-energy-threshold ignition of a lean mixture by an ultrashort-pulsed laser in the filamentation regime, *Light: Sci. Appl.*, 2021, **10**, 49.

33 Y. Petit, S. Henin, J. Kasparian and J. P. Wolf, Production of ozone and nitrogen oxides by laser filamentation, *Appl. Phys. Lett.*, 2010, **97**, 021108.

34 A. Camino, S. Li, Z. Hao and J. Lin, Spectroscopic determination of NO_2, NO_3 and O_3 temporal evolution induced by femtosecond filamentation in air, *Appl. Phys. Lett.*, 2015, **106**, 021105.

35 X.-D. Huang, M. Zhang, L.-H. Deng, S.-B. Pang, K. Liu and H.-L. Xu, Measurement of CO, HCN, and NO productions in

This journal is © the Owner Societies 2026

Phys. Chem. Chem. Phys., 2026, **28**, 2976–2985 | **2983**

atmospheric reaction induced by femtosecond laser filament, *Chin. Phys. B*, 2022, **31**, 097801.

36 A. du Plessis, C. A. Strydom, H. Uys and L. R. Botha, Laser induced and controlled chemical reaction of carbon monoxide and hydrogen, *J. Chem. Phys.*, 2011, **135**, 204303.

37 F. Valle, C. Salgado, J. I. Apinaniz, A. V. Carpentier, M. S. Albaneda and L. Roso, *et al.*, Determination of the species generated in atmospheric-pressure laser-induced plasmas by mass spectrometry techniques, *Laser Phys.*, 2016, **26**, 055602.

38 A. Matsuda, K. Tani, Y. Takeuchi, Y. Hayakawa and A. Hishikawa, Association reaction of gaseous C_2H_4 in femtosecond laser filaments studied by time-of-flight mass spectrometry, *ACS Omega*, 2021, **6**, 29862–29868.

39 J. Peng, N. Puskas, P. B. Corkum, D. M. Rayner and A. V. Loboda, High-pressure gas phase femtosecond laser ionization mass spectrometry, *Anal. Chem.*, 2012, **84**, 5633–5640.

40 NIST Mass Spectroscopy Data Center, W. E. Wallace, director, in *Mass Spectra in NIST Chemistry WebBook, NIST Standard Reference Database Number 69*, ed. P. J. Linstrom and W. G. Mallard, Gaithersburg MD, National Institute of Standards and Technology, 2025.

41 M. Castillejo, S. Couris, E. Koudoumas and M. Martin, Ionization and fragmentation of aromatic and single-bonded hydrocarbons with 50 fs laser pulses at 800 nm, *Chem. Phys. Lett.*, 1999, **308**, 373–380.

42 K. Hoshina, T. Shirota and M. Tsuge, Two-body metastable dissociation of *n*-pentane and *n*-hexane triplet dications in intense femtosecond-laser fields, *J. Phys. Chem. A*, 2021, **125**, 9508–9517.

43 W. C. Wiley and I. H. McLaren, Time-of-flight mass spectrometer with improved resolution, *Rev. Sci. Instrum.*, 1955, **26**, 1150–1157.

44 H. Hasegawa, A. Hishikawa and K. Yamanouchi, Coincidence imaging of Coulomb explosion of CS_2 in intense laser fields, *Chem. Phys. Lett.*, 2001, **349**, 57–63.

45 M. V. Ammosov, N. B. Delone and V. P. Krainov, Tunnel ionization of complex atoms and of atomic ions in an alternating electromagnetic field, *J. Exp. Theor. Phys.*, 1986, **64**, 1191–1194.

46 X. M. Tong, Z. X. Zhao and C. D. Lin, Theory of molecular tunneling ionization, *Phys. Rev. A:At., Mol., Opt. Phys.*, 2002, **66**, 033402.

47 P. Walch, M. Mahieu, L. Arantchouk, Y. B. André, A. Mysyrowicz and A. Houard, Cumulative air density depletion during high repetition rate filamentation of femtosecond laser pulses: Application to electric discharge triggering, *Appl. Phys. Lett.*, 2021, **119**, 264101.

48 K. Linsuain, A. K. Shaik, M. P. Polek and S. S. Harilal, Impact of ultrafast laser pulse repetition rate on flament acoustic and emission signatures, *J. Appl. Phys.*, 2025, **137**, 173307.

49 A. V. Bulgakov, I. Mirza, N. M. Bulgakova, V. P. Zhukov, R. Machulka and O. Haderka, *et al.*, Initiation of air ionization by ultrashort laser pulses: Evidence for a role of

metastable-state air molecules, *J. Phys. D: Appl. Phys.*, 2018, **51**, 25LT02.

50 S. Xu, X. Sun, B. Zeng, W. Chu, J. Zhao and W. Liu, *et al.*, Simple method of measuring laser peak intensity inside femtosecond laser filament in air, *Opt. Express*, 2012, **20**, 299–307.

51 A. Becker, N. Aközbek, K. Vijayalakshimi, E. Oral, C. M. Bowden and S. L. Chin, Intensity clamping and re-focusing of intense femtosecond laser pulses in nitrogen molecular gas, *Appl. Phys. B:Lasers Opt.*, 2001, **73**, 287–290.

52 A. A. Ionin, S. I. Kudryashov, S. V. Makarov, L. V. Seleznev and D. V. Sinitsyn, Multiple filamentation of intense femtosecond laser pulses in air, *JETP Lett.*, 2009, **90**, 423–427.

53 A. Talebpour, A. D. Bandrauk, J. Yang and S. L. Chin, Multiphoton ionization of inner-valence electrons and fragmentation of ethylene in an intense Ti:sapphire laser system, *Chem. Phys. Lett.*, 1999, **313**, 789–794.

54 S. G. Lias, in *Ionization Energy Evaluation in NIST Chemistry WebBook, NIST Standard Reference Database Number 69*, ed. P. J. Linstrom and W. G. Mallard, Gaithersburg MD, National Institute of Standards and Technology, 2025.

55 E. H. Wilson and S. K. Atreya, Chemical sources of haze formation in Titan's atmosphere, *Planet. Space Sci.*, 2003, **51**, 1017–1033.

56 X. Gu, Y. S. Kim, R. I. Kaiser, A. M. Mebel, M. C. Liang and Y. L. Yung, Chemical dynamics of triacetylene formation and implications to the synthesis of polyynes in Titan's atmosphere, *Proc. Natl. Acad. Sci. U. S. A.*, 2009, **106**, 16078–16083.

57 C. Berteloite, S. D. L. Picard, N. Balucani, A. Canosa and I. R. Sims, Low temperature rate coefficients for reactions of the butadiynyl radical, C_4H, with various hydrocarbons. Part I: reactions with alkanes (CH_4, C_2H_6, C_3H_8, C_4H_{10}), *Phys. Chem. Chem. Phys.*, 2010, **12**, 3666–3676.

58 C. Berteloite, S. D. L. Picard, N. Balucani, A. Canosa and I. R. Sims, Low temperature rate coefficients for reactions of the butadiynyl radical, C_4H, with various hydrocarbons. Part II: reactions with alkenes (ethylene, propene, 1-butene), dienes (allene, 1,3-butadiene), and alkynes (acetylene, propyne and 1-butyne), *Phys. Chem. Chem. Phys.*, 2010, **12**, 3677–3689.

59 Y. L. Sun, W. J. Huang and S. H. Lee, Formation of polyynes C_4H_2, C_6H_2, C_8H_2, and $C_{10}H_2$ from reactions of C_2H, C_4H, C_6H, and C_8H radicals with C_2H_2, *J. Phys. Chem. Lett.*, 2015, **6**, 4117–4122.

60 Y. L. Sun, W. J. Huang and S. H. Lee, Formation of C_3H_2, C_5H_2, C_7H_2, and C_9H_2 from reactions of CH, C_3H, C_5H, and C_7H radicals with C_2H_2, *Phys. Chem. Chem. Phys.*, 2016, **18**, 2120–2129.

61 Y. L. Sun, W. J. Huand and S. H. Lee, Formation of octatetrayne (HC_8H) from the reaction of butadiynil (C_4H) with butadiyne (HC_4H), *Chem. Phys. Lett.*, 2017, **690**, 147–152.

62 Y. L. Sun, W. J. Huang and S. H. Lee, Formation of C_9H_2 and $C_{10}H_2$ from reactions $C_3H + C_6H_2$ and $C_4H + C_6H_2$, *J. Phys. Chem. A*, 2017, **121**, 9687–9697.

63 I. A. Medvedkov, Z. Yang, A. A. Nikolayev, S. J. Goettl, A. K. Eckhardt and A. M. Mebel, *et al.*, Binding the power of cycloaddition and cross-coupling in a single mechanism:

2984 | *Phys. Chem. Chem. Phys.*, 2026, **28**, 2976–2985

This journal is © the Owner Societies 2026

An unexpected bending journey to radical chemistry of butadiynyl with conjugated dienes, *J. Phys. Chem. Lett.*, 2025, **16**, 658–666.

64 X. Gu, Y. Guo and R. I. Kaiser, Mass spectrum of the butadiynyl radical (C_4H; $X^2\Sigma^+$), *Int. J. Mass Spectrom.*, 2005, **246**, 29–34.

65 C. A. Arrington, C. Ramos, A. D. Robinson and T. S. Zwier, Ultraviolet photochemistry of diacetylene with alkynes and alkenes: Spectroscopic characterization of the products, *J. Phys. Chem. A*, 1999, **103**, 1294–1299.

66 K. Sugiyama, T. Fujii, M. Miki, M. Yamaguchi, A. Zhidkov and E. Hotta, *et al.*, Laser-filament-induced corona discharges and remote measurements of electric fields, *Opt. Lett.*, 2009, **34**, 2964–2966.

67 T. R. Taylor, C. Xu and D. M. Neumark, Photoelectron spectra of the $C_{2n}H^-$ ($n = 1$–4) and $C_{2n}D^-$ ($n = 1$–3) anions, *J. Chem. Phys.*, 1998, **108**, 10018–10026.

68 B. Bastian, T. Michaelsen, J. Meyer and R. Wester, Anionic carbon chain growth in reactions of C_2^-, C_4^-, C_6^-, C_2H^-, C_4H^-, and C_6H^- with C_2H_2, *Astrophys. J.*, 2019, **878**, 162.

69 V. Vuitton, P. Lavvas, R. V. Yelle, M. Galand, A. Wellbrock, G. R. Lewis, A. J. Coates and J.-E. Wahlund, Negative ion chemistry in Titan's upper atmosphere, *Planet. Space Sci.*, 2009, **57**, 1558–1572.

70 C. S. Casari, M. Tommasini, R. R. Tykwinski and A. Milani, Carbon-atom wires: 1-D systems with tunable properties, *Nanoscale*, 2016, **8**, 4414–4435.

71 S. Peggiani, A. Senis, A. Facibeni, A. Milani, P. Serafini and G. Cerrato, *et al.*, Size-selected polyynes synthesized by submerged arc discharge in water, *Chem. Phys. Lett.*, 2020, **740**, 137054.

72 R. I. Kaiser, Experimental investigation on the formation of carbon-bearing molecules in the interstellar medium via neutral-neutral reactions, *Chem. Rev.*, 2002, **102**, 1309–1358.

This journal is © the Owner Societies 2026

Phys. Chem. Chem. Phys., 2026, **28**, 2976–2985 | **2985**